Highly Promoted Photocatalytic Hydrogen Generation by Multiple Electron Transfer Pathways

Xiaojiao Yuan, Cong Wang, Diana Dragoe, Patricia Beaunier, Christophe Colbeau-Justin, Hynd Remita

Highly Promoted Photocatalytic Hydrogen Generation by Efficient Multiple Electron Transfer Pathways

Xiaojiao Yuan[1], Cong Wang[1], Diana Dragoe[2], Patricia Beaunier[3], Christophe Colbeau-Justin[1], Hynd Remita[1,4*]

[1] Institut de Chimie Physique, UMR 8000 CNRS, Université Paris-Saclay, 91405 Orsay, France

[2] Institut de Chimie Moléculaire et des Matériaux d'Orsay, Université Paris-Saclay, 91405 Orsay, France

[3] Sorbonne Université, CNRS, UMR 7197, Laboratoire de Réactivité de Surface, 75005 Paris, France

[4] CNRS, Institut de Chimie Physique, UMR 8000, 91405 Orsay, France

E-mail : hynd.remita@universite-paris-saclay.fr

Abstract

A facile development of highly efficient photocatalytic nanostructures for solar fuel production via controlled cocatalyst deposition is described. 2 nm-Pt nanoparticles were selectively synthesized by radiolysis on polypyrrole (PPy), TiO_2 or on both PPy-TiO_2 (noted respectively (Pt-PPy)-TiO_2, (Pt-TiO_2)-PPy and Pt-(PPy-TiO_2)). The PPy nanostructures not only act a photosensitizer, but also as a connection bridge between two light-harvesting semiconductors to form a p-n heterojunction, which absorbs UV and visible light efficiently. The designed heterojunction photocatalyst nanostructures (Pt-(PPy-TiO_2)) exhibit broadened absorption to the visible region, long life-time of charge carriers and high photocatalytic activity for hydrogen production. This activity is markedly enhanced compared with that of (Pt-PPy)-TiO_2 and (Pt-TiO_2)-PPy, and is ascribed to more efficient multiple electron transfer pathways. Such designed structures provide promising ways for selected site deposition of

metal nanoparticles on heterojunction semiconductors in high efficiency conversion from solar energy to solar fuel application.

Keywords: Heterojunction photocatalyst, Hydrogen generation, Polypyrrole, TiO_2, Platinum cocatalyst.

1. Introduction

Hydrogen (H_2) is a considerable green and renewable energy. A lot of attention is presently paid to develop photo- or electro-catalysts to solve environmental issues and to produce solar hydrogen because of its high-energy capacity and environmental friendliness [1]. The photocatalytic hydrogen generation from water splitting with semiconductors under solar irradiation is a promising way to produce hydrogen, which has attracted many researchers to extensively investigate and develop appropriate semiconductor photocatalysts to increase their photocatalytic activity [2-7]. The enhancement of photocatalytic performance is generally owing to a fast transfer of photogenerated electrons from the semiconductor to metal leading to the longer lifetime of the excited charge carriers [8]. Besides, a suitable band gap (< 3.2 eV) and structure of the photocatalysts (heterojunction, p-n junction or phase junction), surface reactivity (doped cocatalysts), particle size and distribution of cocatalysts are also key factors for a photocatalytic reaction [9].

Recently, conjugated polymer nanostructures coupled with narrow band gap and unique π-conjugated electron systems as a new class of photocatalysts have received much attention in various photocatalysis application such as water treatment [10-13] and green H_2 production. [14, 15]. However, the photocatalytic efficiency of pristine conjugated polymers is very low due to their rapid charge carrier recombination and sluggish reaction kinetics. A promising way to increase the photocatalytic property of conjugated polymer-based photocatalysts is their combination with semiconductors such as poly(benzothiadiazole) (BBT) [16], poly(3-hexylthiophene) (P3HT) [17], or polypyrrole (PPy) [18]

modification with titania. Titania composites with conjugated polymers present in general high absorption efficiency in the visible region, less electron-hole recombination, high charge carrier mobility, good stability and excellent biocompatibility. In addition, introducing cocatalysts in conjugated-titania heterostructures can remarkably enhance the photocatalytic efficiency due to the prolonged life time of the charge carriers and increased active sites. Although some conjugated polymer-semiconductor-based ternary structure nanocomposites have successfully constructed such as Pt@TiO_2/g-C_3N_4 [19], CdS/Cu_7S_4/g-C_3N_4 [20], Au/TiO_2(P25)-gC_3N_4 [21], little attention has been paid to considering the multiple electron transfer pathways. Indeed, the multiple electron-transfer pathways are very important for the charge carrier separation and hot electron transfer and accumulation by manipulating deposition cocatalysts on different catalysts in a ternary system [22].

Based on the above considerations, here we successfully fabricated for the first time the ternary hybrid PPy-TiO_2 nanocomposites with small Pt nanoparticles (2 nm) induced by radiolysis, and we controlled the deposition site on PPy, TiO_2 or on both PPy-TiO_2 (noted respectively (Pt-PPy)-TiO_2, (Pt-TiO_2)-PPy and Pt-(PPy-TiO_2)). The photocatalytic performance of the different Pt-modified PPy-TiO_2 composites for hydrogen production under both ultraviolet and visible light irradiation were investigated. The results indicate that Pt-(PPy-TiO_2) structures exhibit significantly enhanced photocatalytic hydrogen production due to more efficient electron separation and transfer compared with (Pt-PPy)-TiO_2 and (Pt-TiO_2)-PPy. Our work provides a promising method for the design of ternary nanostructures of metal-semiconductor-conjugated polymer hybrids with high photocatalytic activity for production of solar fuels.

2. Experimental Section

2.1. Materials Preparation

PPy nanostructures were synthesized by chemical polymerization according to our previous work. In brief, hexagonal mesophases used as soft template were made of a mixture of NaCl (0.2 M), SDS

(sodium dodecyl sulfate, 0.8 g), cyclohexane as oil phase (6 mL) and surfactant (n-pentanol, 400 μL). $FeCl_3$ used as oxidant (0.1 M) was added into the mixture, which was vortexed. PPy nanostructures were obtained by oxidation of Py by Fe^{3+} in the mesophases for 2 h. The mesophase was then destabilized by adding ethanol. Finally, the PPy nanostructures powder was collected by centrifugation, washing and drying [11].

TiO_2 P25 was purchased from Evonik Industries AG (surface area 50 m^2 g^{-1}). The PPy/TiO_2 composite was obtained by putting PPy and TiO_2 in contact under ultrasounds (30 min) in ethanol suspension. Different PPy/TiO_2 mass ratio were obtained. For the photocatalytic tests the optimized mass ratio between PPy and TiO_2 was found to be 1/4.

Radiolysis is a powerful technique to synthesize metal nanoparticles (NPs) of controlled sizes and shapes [23]. Pt NPs were synthesized by radiolysis (using a panoramic ^{60}Co γ source) at a dose rate of 4 kGy h^{-1}. The metal salts or complexes (here $Pt^{II}(acac)_2$ purchased from Aldrich) are reduced by solvated electrons and alcohol radicals induced by solvent radiolysis [14].

In the following preparation of samples process, the samples are using theoretical loading rate of Pt (1wt%). The preparation route of (Pt-PPy)-TiO_2 is the following: Firstly, the PPy nanostructures (20 mg) were added to an ethanolic solution (25 mL) containing platinum acetylacetonate ($5x10^{-5}$ M). The tube containing the dispersion was closed with a septum, degassed with N_2, and then irradiated with γ-rays (^{60}Co γ source). After 30 min irradiation at a dose rate of 4 kGy h^{-1}, the Pt-PPy powder was collected after centrifugation, it was then rinsed with water and ethanol and dried. In a second step, the Pt-PPy composite (20 mg) was mixed with TiO_2 (80 mg) in 25 mL of ethanol under sonication. Finally, the (Pt-PPy)-TiO_2 was dried in the oven at 60 °C for overnight (**Figure 1a**).

Synthesis of (Pt-TiO_2)-PPy. The synthesis procedure of (Pt-TiO_2)-PPy was summarized in **Figure 1b**. The preparation route is similar to that of (Pt-PPy)-TiO_2. The only difference is that, in the first step, TiO_2 (80 mg) was dispersed into 25 mL of an ethanol solution containing the Pt^{II} precursor ($2x10^{-4}$ M). The dispersion was irradiated under N_2 atmosphere. The following steps were the same like the

above mentioned.

Synthesis of Pt-(PPy-TiO_2). PPy (20 mg) were mixed with TiO_2 (80 mg) in an ethanol solution (25 mL) containing platinum acetylacetonate ($2.5x10^{-4}$ M). Then the mixture was sonicated for 10 min to disperse the aggregated nanoparticles and then degassed with N_2. The samples were exposed to γ-rays for 30 min (**Figure. 1c**).

Samples with different loading rates of Pt on PPy-TiO_2 were also synthesized labeled as x%Pt-(PPy-TiO_2).

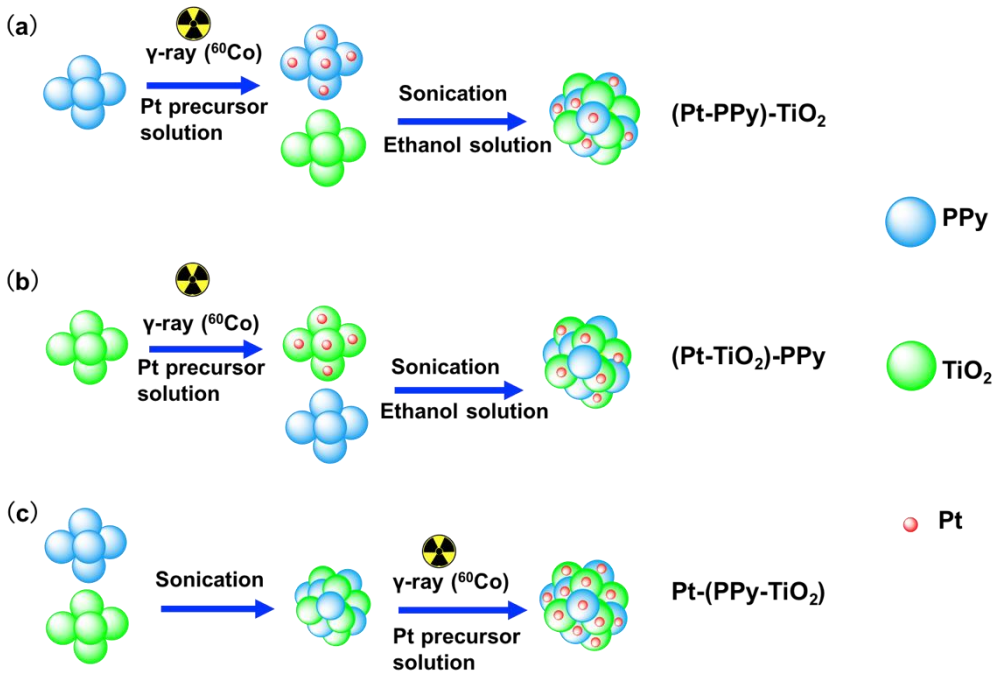

Figure 1. Schemes of modification of TiO_2-PPy with Pt cocatalyst deposited on different sites: on **(a)** PPy, **(b)** TiO_2, and **(c)** PPy-TiO_2.

2.2. Characterizations

Transmission electron microscopy (TEM) (JEOL JEM 2010 UHR operating at 200 kV) was used to observe the morphology and the structures of nanomaterials.

The UV-vis absorption spectra of the samples were recorded with a Cary 5000 Series, Agilent

Technologies.

Time-resolved microwave conductivity (TRMC) technique was applied to investigate the lifetime of charge carrier of photocatalysts under different excitation wavelengths. A pulsed light source (Nd: YAG laser) equipped with an optical parametric oscillator (OPO; EKSPLA, NT342B) was used to excite the samples and a Gunn diode (30 GHz) was used to generate microwaves. The principle of TRMC was described in supporting information [24-26].

X-ray photoelectron spectroscopy (XPS) studies were carried out on an Alpha X-ray Spectrometer with monochromatic Al/Kα under ultrahigh vacuum. C 1s peak (284.6 eV) was used as reference.

The electrochemical measurements were performed in Origalys workstation with a three-electrode system (the prepared sample electrode, counter electrode of Pt foil and a Ag/AgCl electrode as the reference). The working electrodes were prepared by dispersing the samples (3 mg) in ethanol (3 mL) on fluorine doped tin oxide (FTO) substrate. The samples were then dried at room temperature. For photocurrent density with time (*i-t*) curve was recorded at a potential of -200 V. Electrochemical impedance spectra (EIS) were measured in 0.1 M Na_2SO_4 solution with an amplitude of 10 mV, Frequency: 0.1 Hz-1000 Hz at 0.2 V.

2.3. Photocatalytic tests

The photocatalytic activity of the different samples for hydrogen generation under UV and visible light was evaluated. 20 mg of the photocatalyst were dispersed in water-methanol mixture solution (20 mL, $V_{methanol}$/ V_{water} is 1/4) under stirring. The suspension was bubbled with N_2 to remove oxygen and then illuminated under 300 W xenon lamp. For the experiments under visible irradiation, a filter cutting at 420 nm was used. Every 10 min (for UV light) or 1 h (for visible light), 0.2 mL of the gas was taken and injected in the gas chromatograph (GC, Shimadzu GC-14B) instrument to analyze the amount of H_2.

3. Results and Discussion

3.1 Characterizations of photocatalysts

Figure 2 presents the TEM images of Pt-(PPy-TiO_2), (Pt-TiO_2)-PPy, (Pt-PPy)-TiO_2 nanocomposite materials. When the Pt precursor is irradiated in the presence of the PPy-TiO_2 composite, Pt NPs are formed on both TiO_2, on the polymer and at the interface, with a preferential deposition on PPy. The TEM images of Pt-(PPy-TiO_2) present small and monodisperse Pt nanoparticles (black dots, ~2.2 nm, **Figure S1**) on the surface of the PPy-TiO_2 composite (**Figure 2a-b**). The yellow circled parts show preferential deposition of Pt NPs on PPy nanostructures (NSs).

Figure 2c-d shows TEM images of the samples with Pt NPs synthesized on TiO_2 previous to the heterojunction with PPy: 2 nm Pt NPs uniformly dispersed on the TiO_2 were observed. In addition, Pt NPs were found to deposit at the edges of TiO_2 by radiolytic reduction [27] and Pt NPs were not observed on PPy. **Figure 2e-f** present TEM images of the samples with Pt NPs synthesis on PPy NSs previous to the heterojunction with TiO_2: Pt NPs of homogeneous size were well dispersed on PPy, and no Pt NPs were observed on TiO_2.

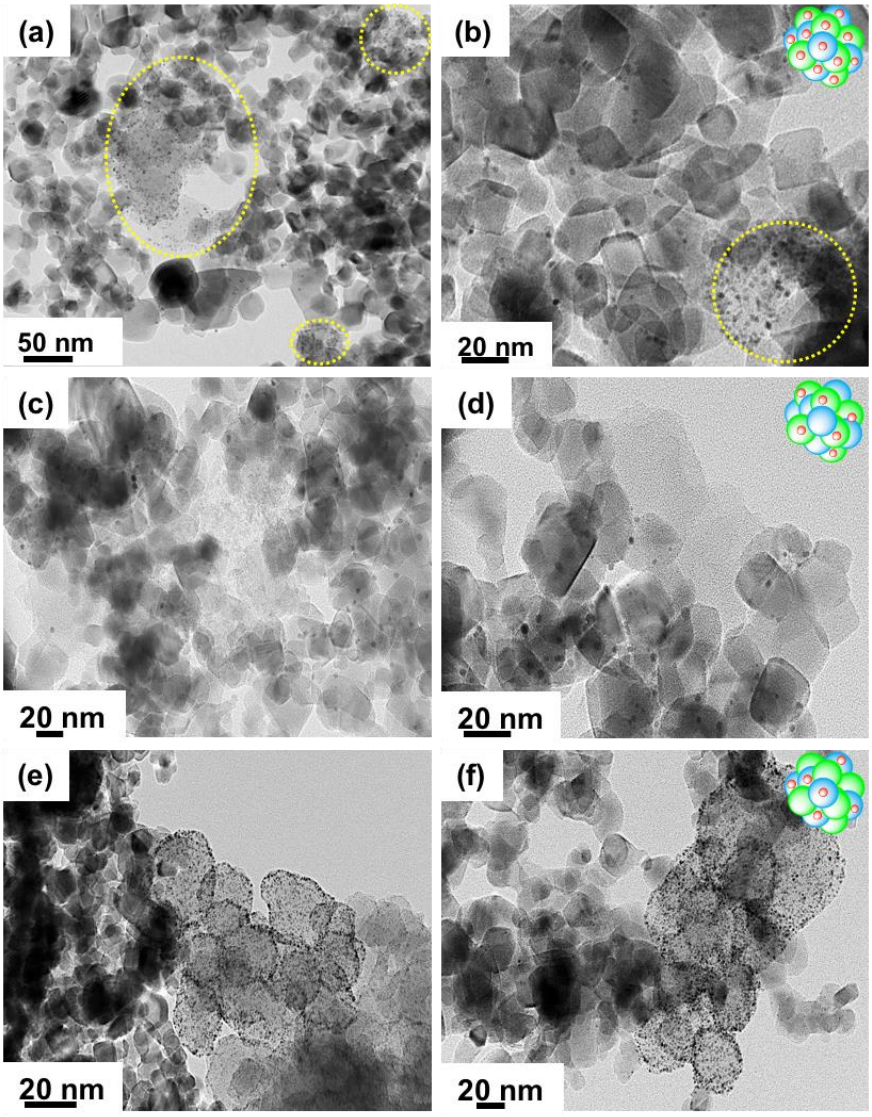

Figure 2. TEM images of **(a-b)** Pt-(PPy-TiO_2), **(c-d)** (Pt-TiO_2)-PPy, **(e-f)** (Pt-PPy)-TiO_2. The mass ratio between PPy and TiO_2 was 1:4 for all the samples.

The UV-vis diffuse reflectance spectra (DRS) of the photocatalysts are shown in **Figure 3a**. The absorption bands from 200 nm to 400 nm are observed owing to the electrons promotion of TiO_2 from valence band (VB) to the conduction band (CB) [28]. Compared with bare TiO_2, Pt-TiO_2 show higher absorption under visible light and red shift (to some extent), which characterize the optical properties of Pt NPs on TiO_2 [29]. Thanks to the strong absorption of PPy in the visible light region, Pt-(PPy-TiO_2) shows high absorption intensity from 400~800 nm, indicating a significantly improved

activation under visible light. Moreover, based on the Kubelka-Munk method, the estimated band gap for TiO_2, Pt-TiO_2 and Pt-(PPy-TiO_2) are 3.20 eV, 3.06 eV and 2.83 eV, respectively (**Figure 3b**). The narrower band gap of Pt-(PPy-TiO_2) is mainly attributed to the heterojunction of titania with PPy nanostructures, which can adsorb more photons to provide more photogenerated charge carriers and improve the photocatalytic property of the photocatalyst. **Figure S2** shows the UV-Vis absorption spectra of (Pt-PPy)-TiO_2, (Pt-TiO_2)-PPy and Pt-(TiO_2-PPy) samples. All these three samples present high absorption in the visible region and the spectra are quite similar. A small difference was observed probably due to the shield of PPy by TiO_2 during the synthesis.

The XRD peaks of the samples correspond to typical anatase and rutile TiO_2 patterns, which match with the PDF card number of 99-0008 (anatase) and 99-0090 (rutile) [31] (**Figure S3**). Because of the small size of Pt NPs, almost no XRD signal of Pt was observed.

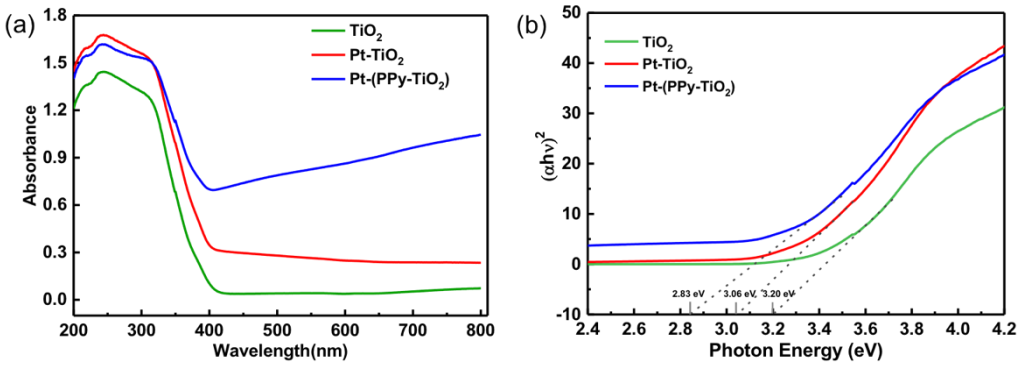

Figure 3. UV-vis absorption spectra **(a)** and Mott-Schottky plot of the as-prepared samples, **(b)** (The mass ratio PPy/TiO_2 was 1:4 for all the samples).

The TRMC technique was used to evaluate the dynamics of charge-carriers in TiO_2-based composites at different wavelengths. **Figure 4a** presents the TRMC signals at 360 nm excitation for pure TiO_2, and its platinized form. Pt NPs accelerate the decay at short time range, and does not modify it at long time range [30]. Pt NPs are known to be a sink for electrons, and a sharp fast decay of the signal for the Pt-modified samples is obtained: Pt NPs deposited on TiO_2 act as electron scavengers

decreasing the recombination of charge-carriers, which is beneficial for the photocatalytic activity [20]. Nevertheless, in our previous work, after introducing PPy in TiO_2, the lower signal decay in PPy-TiO_2 than pristine TiO_2 was obtained, which may be due to PPy shield effect, fast recombination effect, or fast electron trapping [31]. Interestingly, **Figure 4a** evidences that the TRMC signal of Pt-(PPy-TiO_2) is not an addition of separate effects of Pt and PPy. A synergetic influence seems to occur. Indeed, the observed signal is quite flat, with a very slow decay. It indicates a real low amount of fast recombination and free e^- with high lifetime resulting from good charge-carrier separations. Those effects should be favorable to the activity.

Under visible illumination (at 420 and 450 nm), as expected, the TRMC signal is reduced. Pt-(PPy-TiO_2) shows faster decay at very short range time compared to that of Pt-TiO_2 and TiO_2, which indicates more efficient electron trapping and transfer. Moreover, Pt-(PPy-TiO_2) presents a slightly longer lifetime of electrons from the trend of long-rang decay than that of Pt-TiO_2 and TiO_2 (**Figure 4b-c**).

The TRMC signals of (Pt-PPy)-TiO_2, (Pt-TiO_2)-PPy and Pt-(PPy-TiO_2) under UV, at 360 nm, are shown in **Figure 4d**: Unlike Pt-(PPy-TiO_2), the composites (Pt-PPy)-TiO_2 and (Pt-TiO_2)-PPy present a fast-global decay, leading to a really low number of charge-carriers after 0.2 μs. It means that the synergetic effect is only observed on Pt-(PPy-TiO_2), which leads to the most efficient electron transfer and the longest life time of electrons. In (Pt-TiO_2)-PPy and (Pt-PPy)-TiO_2 the fast decay is probably be due to high level of recombination.

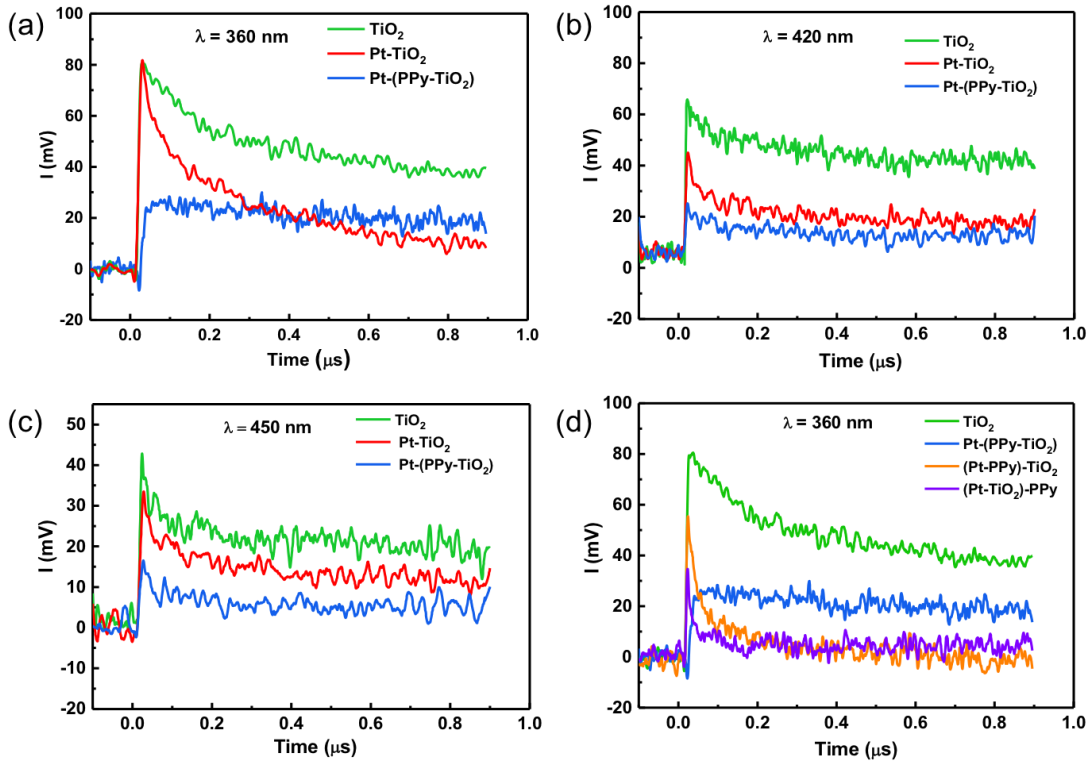

Figure 4. TRMC measurements of Pt-(PPy-TiO_2), Pt-TiO_2 and TiO_2 at 360 nm **(a)**, 420 nm **(b)**, 450 nm **(c)**, respectively. The laser energy of these wavelengths was 1.1, 2.3, 2.3 $mJ \cdot cm^{-2}$. TRMC measurements of (Pt-PPy)-TiO_2, (Pt-TiO_2)-PPy, Pt-(PPy-TiO_2) and TiO_2 at 360 nm (**d**). The mass ratio between PPy and TiO_2 was 1:4 for all the samples and the Pt loading is 1%.

The surface composition and chemical states of (Pt-PPy)-TiO_2, (Pt-TiO_2)-PPy and Pt-(PPy-TiO_2) were studied by XPS spectroscopy (**Figure 5a-d**). The full spectrum of Pt-(PPy-TiO_2) contains the signals of C, N, O, and Pt (**Figure S4**). Pt 4f spectrum of Pt-(PPy-TiO_2) shows that part of Pt in the composite is oxidized. The doublet at 70.78 eV (Pt $4f_{7/2}$) and 73.98 eV (Pt $4f_{5/2}$) corresponds to metallic Pt which are lower than pure metallic Pt (Pt $4f_{7/2}$ = 71.2 eV) due to the electron transfer happens from TiO_2 and PPy to Pt nanoparticles with higher work function [32]. The binding energy at 74.95 eV (Pt $4f_{7/2}$) and 76.41 eV (Pt $4f_{5/2}$) are corresponding to PtO_2, (**Figure 5a**) [33]. Different valence states of Pt nanoparticles can provide higher active sites and more oxygen defects, which is beneficial for surface chemical adsorption and catalysis [19]. The characteristic peaks of Ti $2p_{3/2}$ (458.9 eV) and Ti

$2p_{1/2}$ (464.6 eV) spectrum of (Pt-PPy)-TiO_2, (Pt-TiO_2)-PPy and Pt-(PPy-TiO_2) show a slight shift (0.4 eV) toward higher binding energies compared to pure TiO_2 (458.5 eV, Ti $2p_{3/2}$) (**Figure 5b**). With reference to previous reports on TiO_2 [34, 35], such higher energy shifts suggest the formation of heterojunction and interactions of the ternary compounds [36]. The C 1s signal for the PPy is located at a binding energy of 284.9 eV (C-C), 286.2 eV (C-O) and 289.0 eV (O-C=O), respectively (**Figure 5c**). The N 1s high resolution spectra in **Figure 5d** can be fitted into two peaks, which can be attributed to N-C (399.9 eV) and N-C=O (409.1 eV) [37].

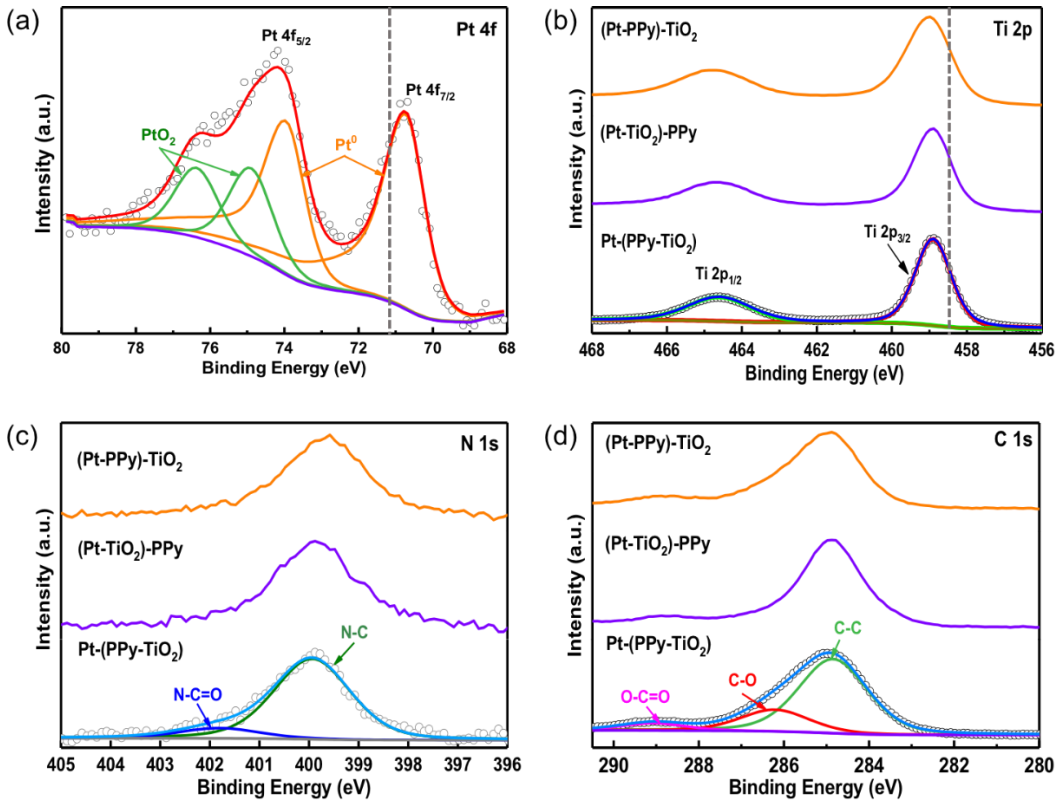

Figure 5 Pt 4f XPS spectra of the Pt-(PPy-TiO_2) **(a)**; Ti 2p **(b)**, C 1s **(c)** and N 1s **(d)** of the (Pt-PPy)-TiO_2, (Pt-TiO_2)-PPy and Pt-(PPy-TiO_2), respectively. The mass ratio between PPy and TiO_2 was 1:4 for all the samples and the Pt loading is 1%.

The transient photocurrent response curves of (Pt-PPy)-TiO_2, (Pt-TiO_2)-PPy and Pt-(PPy-TiO_2) are shown in **Figure 6a**. As expected from the TRMC results, the photocurrent intensity of Pt-(PPy-

TiO_2) is 2.7 times higher than that of (Pt-PPy)-TiO_2 and (Pt-TiO_2)-PPy under AM1.5G, which suggests enhanced efficiency of charge transfer and separation of electron-hole pairs in this sample. Additionally, EIS Nyquist plots were used to explore the interface charge transfer resistances of the electrode materials. The smallest semicircle in EIS for Pt-(PPy-TiO_2) further demonstrated the highest efficient and fastest interfacial charge transfer ability than (Pt-PPy)-TiO_2 and (Pt-TiO_2)-PPy (**Figure 6b**). These results are consistent with TRMC results and strongly support the excellent photocatalytic activity of Pt-(PPy-TiO_2) shown by the following photocatalytic tests.

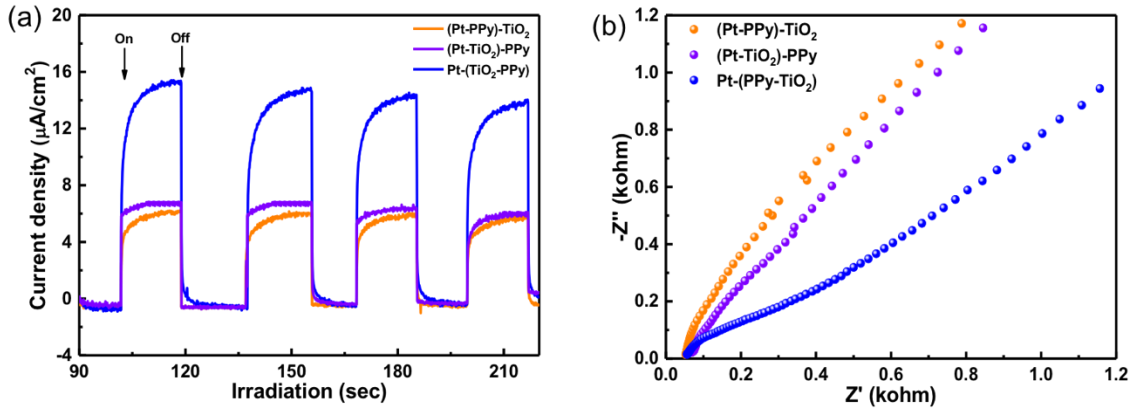

Figure 6. Photocurrent transient **(a)** and Nyquist plots of EIS **(b)** for (Pt-PPy)-TiO_2, (Pt-TiO_2)-PPy and Pt-(PPy-TiO_2) FTO electrodes under UV-vis light irradiation. The mass ratio between PPy and TiO_2 was 1:4 for all the samples and the Pt loading 1%.

3.2 Photocatalytic activity for hydrogen generation

In order to achieve a good photocatalytic activity for hydrogen production, different volume ratios of methanol-water mixture (**Figure S5)**, sacrificial electron donors (**Figure S6)**, and mass ratios of PPy and TiO_2 were investigated (**Figure 7a**). As shown in **Figure S5**, hydrogen production with 1%Pt-(PPy-TiO_2) increased with increasing methanol content until reached to 25%. The photocatalytic activity decreased when the $V_{methanol}/V_{water}$ was more than 25%, and the very low conversion rate was obtained for the case of 100% water or pure methanol. F. Besenbacher et al. revealed a proton-transfer

mechanism that proceeds via an H_3O^+-like transition state, which can explain why the methanol-water mixture presents higher photocatalytic activity compared with pure methanol [38]. The effect of different sacrificial reagents (with the same concentration: 0.2 M) for photocatalytic hydrogen generation was studied (**Figure S6**). We have found that the highest yield of hydrogen was obtained by the use of methanol owing to the partial production of hydrogen through the methanol conversion ($MeOH + H_2O \rightarrow CO_2 + 3H_2$, $\Delta G^0 = 16.1$ kJ/mol) [39]. Furthermore, it is clearly observed that the weight ratio (PPy/TiO_2) has a great influence on hydrogen production (**Figure 7a**). Modification of TiO_2 with a small amount of PPy (maximum 25% in mass) induced an increase in its photoactivity. The photocatalytic activity of 1%Pt-(PPy-TiO_2) is maximum for the PPy/TiO_2 mass ratio 2:8 and decreases drastically with higher ratios. The presence of a large amount of PPy may cover the surface of TiO_2 hindering the light absorption and the injection of excited electrons from the LUMO of PPy to the CB of TiO_2 [40].

Photocatalytic hydrogen evolution experiments were conducted in aqueous solution containing 25% methanol as a hole scavenger. The photocatalyst (1%Pt-(PPy-TiO_2)) is very active for hydrogen production in pure water under UV and visible light. The yield of H_2 production reaches 850.0 µmol and 27.0 µmol after 5 h under UV and visible light irradiation, respectively (**Figure 7b**). As shown in **Figure 7c-d**, 1%Pt-(PPy-TiO_2) exhibits the highest activity for hydrogen production with 125.1 mmol h^{-1} g^{-1} under UV light and 3.2 mmol h^{-1} g^{-1} under visible light irradiation compared with other loading rates of Pt NPs. The hydrogen evolution rate of 1%Pt-(PPy-TiO_2) was greatly enhanced with composite materials with appropriate proportion.

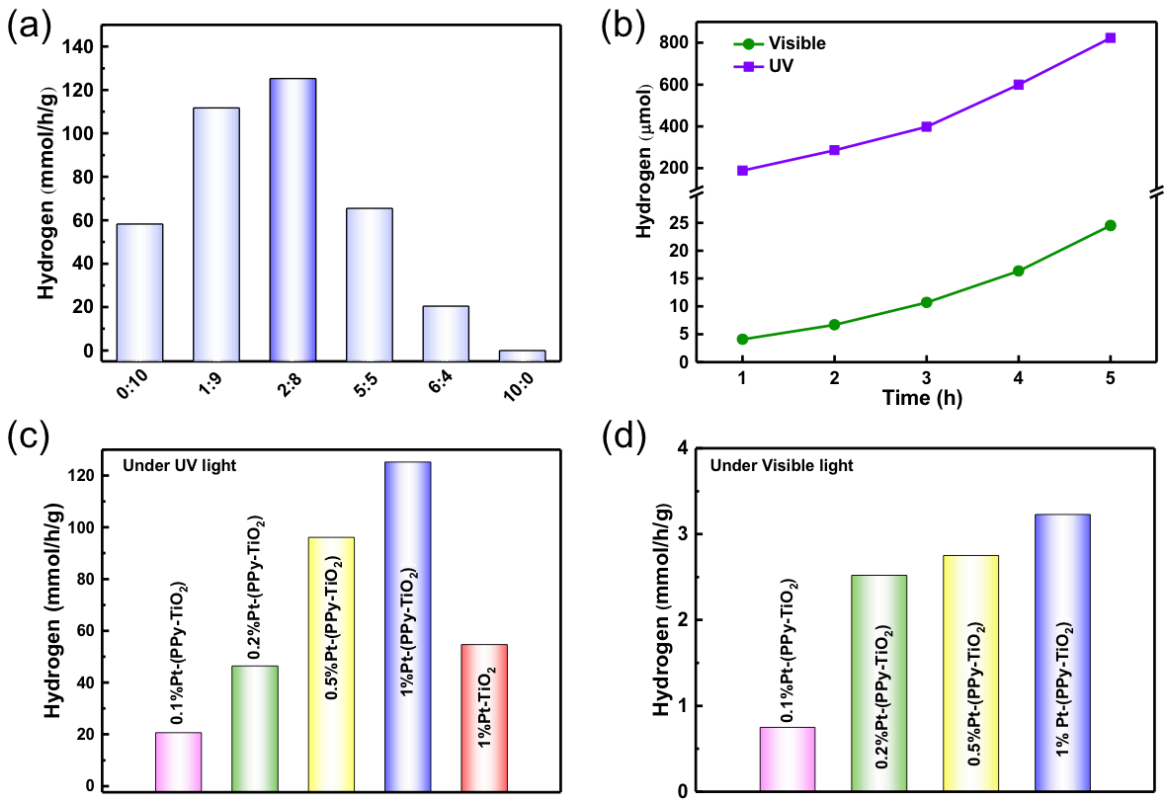

Figure 7. Different mass ratio between PPy and TiO_2 for photocatalytic hydrogen generation **(a)**, Hydrogen production with 1%Pt-(PPy-TiO_2) in pure water under UV and visible light (**b**), hydrogen production with different loading rate of Pt NPs on PPy-TiO_2 (with the fixed mass PPy/TiO_2 ratio 20:80) in methanol-water mixture solution (25% methanol) under both UV light **(c),** and visible light (**d**).

1%Pt-(PPy-TiO_2) photocatalyst shows a significantly enhanced photocatalytic activity for hydrogen generation (125.1 mmol h^{-1} g^{-1} and 3200 μmol h^{-1} g^{-1} under UV and visible light irradiation, respectively) compared with the same loading rate of Pt NPs deposited on PPy (11.8 mmol h^{-1} g^{-1} under UV light and 70.9 μmol h^{-1} g^{-1} under visible light, respectively) and TiO_2 (24.2 mmol h^{-1} g^{-1} under UV and 454.2 μmol h^{-1} g^{-1} under visible light irradiation), respectively (**Figure 8a**). The higher photocatalytic activity of Pt NPs deposited on PPy-TiO_2 can be ascribed to the routes of effective electron transfer ($e^-_{PPy(LUMO)} \rightarrow$Pt and $e^-_{PPy(LUMO)} \rightarrow TiO_{2(CB)} \rightarrow$Pt) compared with (Pt-PPy)-TiO_2 and (Pt-TiO_2)-PPy. Other photocatalysts for hydrogen production have been compared in **Table S1**. Our

photocatalyst Pt-(PPy-TiO_2) is very active for hydrogen production under both UV and visible light, and its performance equal or even surpass the literature reports for photocatalysts based on TiO_2 or PPy (**Table S1**)

For practical applications, it is important to check the stability of the photocatalyst. **Figure 8b** shows that the photocatalyst Pt-(PPy-TiO_2) is stable with cycling.

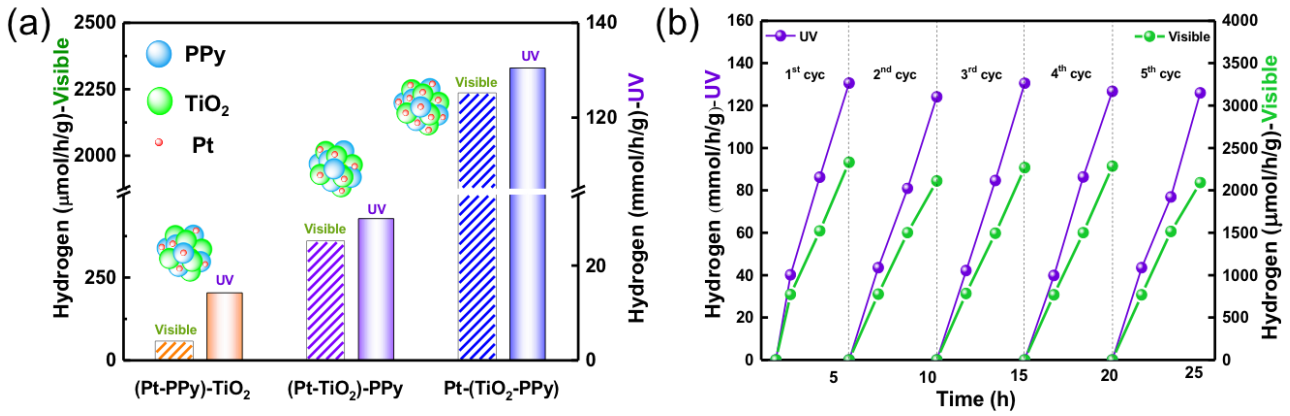

Figure 8. Hydrogen production with (Pt-PPy)-TiO_2, (Pt-TiO_2)-PPy and Pt-(PPy-TiO_2) in methanol-water mixture solution under UV light and visible irradiation **(a)**; The photocatalytic hydrogen production of Pt-(PPy-TiO_2) with cycling in methanol-water mixture solution (25% methanol) (**b**).

3.3 Electron transfer mechanism of (Pt-PPy)-TiO_2, (Pt-TiO_2)-PPy and Pt-(PPy-TiO_2)

The migration of electrons under visible-light in the ternary photocatalysts can be explained by the proposed mechanism in **Figure 9**. Firstly, photocatalytic hydrogen generation involves three main steps: (*i*) light absorption, (*ii*) charge carriers generation and charge transfer to the surface of photocatalysts, and (*iii*) surface redox reactions [41]. Here, PPy as a photosensitizer was used to absorb the incident light to generate e^- and h^+. Pt NPs used as a cocatalysts not only serve as sinks for electrons, but also provide proton reductive sites, and centers for $H^{\cdot}$ radical recombination leading to H_2 formation [14]. In addition, thanks to the suitable CB and VB potential positions of PPy and TiO_2, we could design this very active composite photocatalyst. The energy band structures are described in SI.

As shown in **Figure 9a**, for the (Pt-PPy)-TiO_2 system, the photogenerated electrons in the LUMO

of PPy transfer to Pt NPs of PPy surface and also to TiO_2 CB. Although for (Pt-PPy)-TiO_2 two electron transfer pathways are proposed, its photocatalytic activity is much lower than Pt-(PPy-TiO_2) because the protons can be reduced into $H^{\cdot}$ on the surface of Pt much more efficiently than on bare TiO_2. Pt NPs help also to form H-H bond to lead to H_2. In addition, TRMC signals and photocatalytic tests for H_2 generation indicate that the electron could transfer from PPy to TiO_2, the LUMO of PPy being situated at higher energy position than the CB of TiO_2 [31]. The oxidation of an electron donor (such as methanol) with h^+ happened on the HOMO of PPy ($MeOH \rightarrow 3H_2 + CO_2$).

In (Pt-TiO_2)-PPy ternary system, PPy is introduced to create electrons from the HOMO to LUMO under visible light illumination (**Figure 9b**). The photo-induced electrons migration from PPy to the TiO_2 CB due to the position of the PPy LUMO is much more negative than that of TiO_2, and are eventually injected into the low Fermi level of Pt. As a result, rapid charge separation and slow charge recombination occurred, which results in a good photocatalytic performance. This electron transfer scheme is also illustrated in other ternary systems such as PPy-Ag-TiO_2 [40], TiO_2/CuO/Cu [42], In_2O_3-TiO_2-Pt [43].

More interestingly, the Pt-(PPy-TiO_2) composite shows the best photocatalytic activity compared with (Pt-PPy)-TiO_2 and (Pt-TiO_2)-PPy, because the active Pt sites coexist in both PPy and TiO_2 (as seen in Figure 2a-b). **Figure 9c** illustrates two efficient routes of electron transfer. The excited electrons from PPy LUMO migrate to the surface of PPy and TiO_2, and then are trapped by Pt deposited on PPy and TiO_2 leading to very efficient separation of charge carriers. The most efficient charge carrier separation and transfer in Pt-(PPy-TiO_2) compared with (Pt-PPy)-TiO_2 and (Pt-TiO_2)-PPy were demonstrated by TRMC technique, photoelectrochemical tests and photocatalytic activity. Furthermore, Pt NPs act as a cocatalysts for H^+ reduction and as a site for $H^{\cdot}$ recombination. The synergistic effect of the two electron transfer routes and formation of PPy-TiO_2 heterojunction facilitate the photocatalytic reaction process.

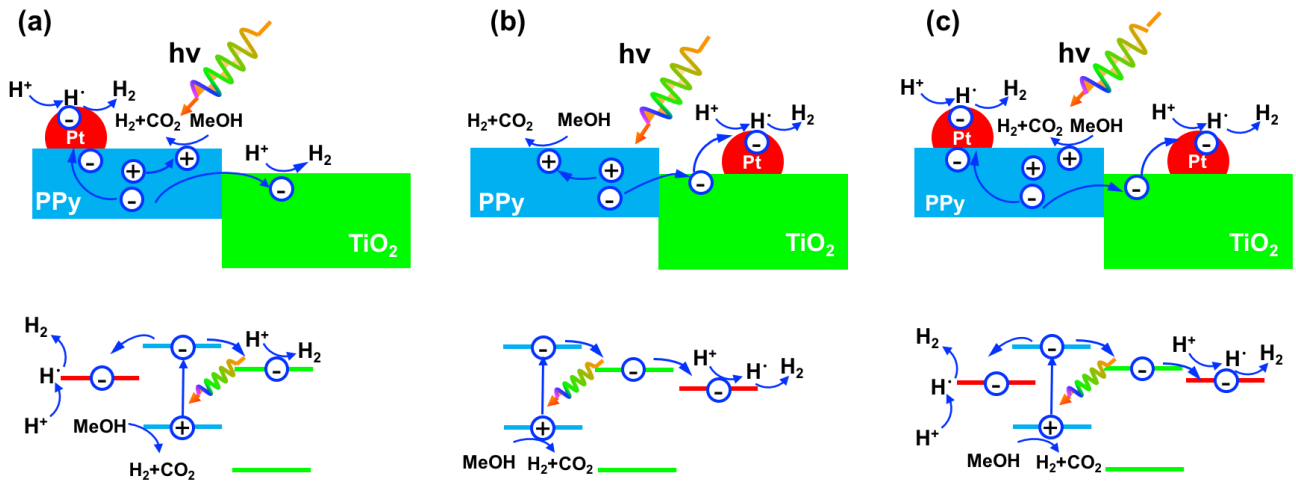

Figure 9. Scheme representation of the electron transfer, migration and hydrogen production mechanism in the hybrid photocatalysts: **(a)** (1%Pt-PPy)-TiO_2; **(b)** (1%Pt-TiO_2)-PPy; **(c)** 1%Pt-(PPy-TiO_2)

4. Conclusions

In summary, different ternary nanostructures based on PPy-TiO_2 composites with controlled site modification with Pt nanoparticles were designed. The photocatalytic activity of Pt-(PPy-TiO_2) for hydrogen generation under UV and visible light is very high and drastically surpasses those of (Pt-PPy)-TiO_2, (Pt-TiO_2)-PPy and Pt-TiO_2. With modification of both PPy and TiO_2 surface with Pt NPs, an efficient electron transfer from PPy to Pt NPs and through TiO_2 to Pt were achieved, which leads to higher charge carriers' separation and accumulation of electrons for the Pt-(PPy-TiO_2) compared with (Pt-PPy)-TiO_2 and (Pt-TiO_2)-PPy. More electrons are driven by and to the Pt nanoparticles, which also act as cocatalysts for H^+ reduction and H-H bond formation. The Pt-(TiO_2-PPy) photocatalyst is stable with cycling. This composite may find promising applications in solar fuels generation. This study will open perspectives in the rational design of ternary composites to facilitate charge transfer for high efficient conversion of solar to chemical energy.

Acknowledgements

X.Y. gratefully acknowledges the financial support from China Scholarship Council (CSC). This work was supported by the IDEX Paris-Saclay and IRS MOMENTOM. J. Li for his help and M.N. Ghazzal for the access to the photoelectrochemical cell he developed. The authors thank Sylvain Franger for access to XRD characterization and Isabelle Lampre for her help.

Reference

[1] L. Liu, X. Zhang, L. Yang, L. Ren, D. Wang, J. Ye, Metal nanoparticles induced photocatalysis, National Science Review, 4 (2017) 761-780.

[2] J. Zhang, Z. Yu, Z. Gao, H. Ge, S. Zhao, C. Chen, S. Chen, X. Tong, M. Wang, Z. Zheng, Porous TiO_2 nanotubes with spatially separated platinum and CoO_x cocatalysts produced by atomic layer deposition for photocatalytic hydrogen production, Angewandte Chemie International Edition, 56 (2017) 816-820.

[3] C. Wang, J. Li, E. Paineau, A. Laachachi, C. Colbeau-Justin, H. Remita, M.N. Ghazzal, A sol–gel biotemplating route with cellulose nanocrystals to design a photocatalyst for improving hydrogen generation, Journal of Materials Chemistry A, 8 (2020) 10779-10786.

[4] J. Li, X. Gao, L. Zhu, M.N. Ghazzal, J. Zhang, C.-H. Tung, L.-Z. Wu, Graphdiyne for crucial gas involved catalytic reactions in energy conversion applications, Energy & Environmental Science, 12 (2020) 1326-1346.

[5] J. Fang, Y. Chen, W. Wang, L. Fang, C. Lu, C. Zhu, J. Kou, Y. Ni, Z. Xu, Highly efficient photocatalytic hydrogen generation of g-C_3N_4-CdS sheets based on plasmon-enhanced triplet–triplet annihilation upconversion, Applied Catalysis B: Environmental, 258 (2019) 117762.

[6] K. Zhu, M. Zhang, X. Feng, L. Qin, S.-Z. Kang, X. Li, A novel copper-bridged graphitic carbon nitride/porphyrin nanocomposite with dramatically enhanced photocatalytic hydrogen generation, Applied Catalysis B: Environmental, 268 (2020) 118434.

[7] Y. Hu, X. Hao, Z. Cui, J. Zhou, S. Chu, Y. Wang, Z. Zou, Enhanced photocarrier separation in conjugated polymer engineered CdS for direct Z-scheme photocatalytic hydrogen evolution, Applied Catalysis B: Environmental, 260 (2020) 118131.

[8] J.B. Joo, R. Dillon, I. Lee, Y. Yin, C.J. Bardeen, F. Zaera, Promotion of atomic hydrogen recombination as an alternative to electron trapping for the role of metals in the photocatalytic production of H_2, Proceedings of the National Academy of Sciences, 111 (2014) 7942-7947.

[9] Q. Zhang, Z. Li, S. Wang, R. Li, X. Zhang, Z. Liang, H. Han, S. Liao, C. Li, Effect of redox cocatalysts location on photocatalytic overall water splitting over cubic $NaTaO_3$ semiconductor crystals exposed with equivalent facets, ACS Catalysis, 6 (2016) 2182-2191.

[10] S. Ghosh, N.A. Kouamé, L. Ramos, S. Remita, A. Dazzi, A. Deniset-Besseau, P. Beaunier, F. Goubard, P.-H. Aubert, H. Remita, Conducting polymer nanostructures for photocatalysis under visible light, Nature Materials, 14 (2015) 505-511.

[11] X. Yuan, D. Floresyona, P.-H. Aubert, T.-T. Bui, S. Remita, S. Ghosh, F. Brisset, F. Goubard, H. Remita, Photocatalytic degradation of organic pollutant with polypyrrole nanostructures under UV and visible light, Applied Catalysis B: Environmental, 242 (2019) 284-292.

[12] D. Floresyona, F. Goubard, P.-H. Aubert, I. Lampre, J. Mathurin, A. Dazzi, S. Ghosh, P. Beaunier, F. Brisset, S. Remita, L. Ramos, R. Hynd, Highly active poly (3-hexylthiophene) nanostructures for photocatalysis under solar light, Applied Catalysis B: Environmental, 209 (2017) 23-32.

[13] S. Ghosh, N.A. Kouame, S. Remita, L. Ramos, F. Goubard, P.-H. Aubert, A. Dazzi, A. Deniset-Besseau, H. Remita, Visible-light active conducting polymer nanostructures with superior photocatalytic activity, Scientific Reports, 5 (2015) 1-9.

[14] X. Yuan, D. Dragoe, P. Beaunier, D.B. Uribe, L. Ramos, M.G. Méndez-Medrano, H. Remita, Polypyrrole nanostructures modified with mono-and bimetallic nanoparticles for photocatalytic H_2 generation, Journal of Materials Chemistry A, 8 (2020) 268-277.

[15] S. Ghosh, S.R. Keshri, S. Bera, R.N. Basu, Enhanced solar hydrogen generation using Cu–Cu_2O integrated polypyrrole nanofibers as heterostructured catalysts, International Journal of Hydrogen Energy, 45 (2020) 6159-6173.

[16] H.-J. Hou, X.-H. Zhang, D.-K. Huang, X. Ding, S.-Y. Wang, X.-L. Yang, S.-Q. Li, Y.-G. Xiang, H. Chen, Conjugated microporous poly (benzothiadiazole)/TiO_2 heterojunction for visible-light-driven H_2 production and pollutant removal, Applied Catalysis B: Environmental, 203 (2017) 563-571.

[17] D. Wang, J. Zhang, Q. Luo, X. Li, Y. Duan, J. An, Characterization and photocatalytic activity of poly (3-hexylthiophene)-modified TiO_2 for degradation of methyl orange under visible light, Journal of Hazardous Materials, 169 (2009) 546-550.

[18] N.M. Dimitrijevic, S. Tepavcevic, Y. Liu, T. Rajh, S.C. Silver, D.M. Tiede, Nanostructured TiO_2/polypyrrole for visible light photocatalysis, The Journal of Physical Chemistry C, 117 (2013) 15540-15544.

[19] Y. Zou, B. Yang, Y. Liu, Y. Ren, J. Ma, X. Zhou, X. Cheng, Y. Deng, Controllable Interface-Induced Co-Assembly toward Highly Ordered Mesoporous Pt@TiO_2/g-C_3N_4 Heterojunctions with Enhanced Photocatalytic Performance, Advanced Functional Materials, 28 (2018) 1806214.

[20] J. Chu, X. Han, Z. Yu, Y. Du, B. Song, P. Xu, Highly efficient visible-light-driven photocatalytic hydrogen production on CdS/Cu_7S_4/g-C_3N_4 ternary heterostructures, ACS Applied Materials & Interfaces, 10 (2018) 20404-20411.
[21] P. Jiménez-Calvo, V. Caps, M.N. Ghazzal, C. Colbeau-Justin, V. Keller, Au/TiO_2 (P25)-gC_3N_4 composites with low gC_3N_4 content enhance TiO_2 sensitization for remarkable H_2 production from water under visible-light irradiation, Nano Energy, (2020) 104888.
[22] K. Zhang, J.H. Cha, S.Y. Jeon, K.O. Kirlikovali, M. Ostadhassan, V. Rasouli, O.K. Farha, H.W. Jang, R.S. Varma, M. Shokouhimehr, Pd modified prussian blue frameworks: Multiple electron transfer pathways for improving catalytic activity toward hydrogenation of nitroaromatics, Molecular Catalysis, 492 (2020) 110967.
[23] M. Klein, J. Nadolna, A. Gołąbiewska, P. Mazierski, T. Klimczuk, H. Remita, A. Zaleska-Medynska, The effect of metal cluster deposition route on structure and photocatalytic activity of mono-and bimetallic nanoparticles supported on TiO_2 by radiolytic method, Applied Surface Science, 378 (2016) 37-48.
[24] A.L. Luna, D. Dragoe, K. Wang, P. Beaunier, E.K. Kowalska, B. Ohtani, D. Bahena Uribe, M.A. Valenzuela, H. Remita, C. Colbeau-Justin, Photocatalytic Hydrogen Evolution Using Ni-Pd/TiO_2: Correlation of Light Absorption, Charge-Carrier Dynamics and Quantum Efficiency, The Journal of Physical Chemistry C, 121 (2017) 14302-14311.
[25] A.L. Luna, E. Novoseltceva, E. Louarn, P. Beaunier, E. Kowalska, B. Ohtani, M.A. Valenzuela, H. Remita, C. Colbeau-Justin, Synergetic effect of Ni and Au nanoparticles synthesized on titania particles for efficient photocatalytic hydrogen production, Applied Catalysis B: Environmental, 191 (2016) 18-28.
[26] M. Méndez-Medrano, E. Kowalska, A. Lehoux, A. Herissan, B. Ohtani, S. Rau, C. Colbeau-Justin, J. Rodríguez-López, H. Remita, Surface Modification of TiO_2 with Au Nanoclusters for Efficient Water Treatment and Hydrogen Generation under Visible Light, The Journal of Physical Chemistry C, 120 (2016) 25010-25022.
[27] N. Roy, K.T. Leung, D. Pradhan, Nitrogen doped reduced graphene oxide based Pt–TiO_2 nanocomposites for enhanced hydrogen evolution, The Journal of Physical Chemistry C, 119 (2015) 19117-19125.
[28] X. Li, P. Wang, B. Huang, X. Qin, X. Zhang, Q. Zhang, X. Zhu, Y. Dai, Precisely locate Pd-Polypyrrole on TiO_2 for enhanced hydrogen production, International Journal of Hydrogen Energy, 42 (2017) 25195-25202.
[29] E. Kowalska, H. Remita, C. Colbeau-Justin, J. Hupka, J. Belloni, Modification of titanium dioxide with platinum ions and clusters: application in photocatalysis, The Journal of Physical Chemistry C,

112 (2008) 1124-1131.
[30] C.A. Emilio, M.I. Litter, M. Kunst, M. Bouchard, C. Colbeau-Justin, Phenol photodegradation on platinized-TiO_2 photocatalysts related to charge-carrier dynamics, Langmuir, 22 (2006) 3606-3613.
[31] X. Yuan, M.P. Kobylanski, Z. Cui, J. Li, P. Beaunier, D. Dragoe, C. Colbeau-Justin, A. Zaleska-Medynska, H. Remita, Highly Active Composite TiO_2-Polypyrrole Nanostructures for Water and Air Depollution Under Visible Light Irradiation, Journal of Environmental Chemical Engineering, 8 (2020) 104178.
[32] Y. Wang, X. Shang, J. Shen, Z. Zhang, D. Wang, J. Lin, J.C. Wu, X. Fu, X. Wang, C. Li, Direct and indirect Z-scheme heterostructure-coupled photosystem enabling cooperation of CO_2 reduction and H_2O oxidation, Nature Communications, 11 (2020) 1-11.
[33] L.K. Ono, J.R. Croy, H. Heinrich, B. Roldan Cuenya, Oxygen chemisorption, formation, and thermal stability of Pt oxides on Pt nanoparticles supported on SiO_2/Si (001): size effects, The Journal of Physical Chemistry C, 115 (2011) 16856-16866.
[34] U. Diebold, T. Madey, TiO_2 by XPS, Surface Science Spectra, 4 (1996) 227-231.
[35] P. Stefanov, M. Shipochka, P. Stefchev, Z. Raicheva, V. Lazarova, L. Spassov, XPS characterization of TiO_2 layers deposited on quartz plates, Journal of Physics: Conference Series, IOP Publishing, 2008, pp. 012039.
[36] J. Yan, H. Wu, H. Chen, Y. Zhang, F. Zhang, S.F. Liu, Fabrication of TiO_2/C_3N_4 heterostructure for enhanced photocatalytic Z-scheme overall water splitting, Applied Catalysis B: Environmental, 191 (2016) 130-137.
[37] J. Cao, Y. Wang, J. Chen, X. Li, F.C. Walsh, J.-H. Ouyang, D. Jia, Y. Zhou, Three-dimensional graphene oxide/polypyrrole composite electrodes fabricated by one-step electrodeposition for high performance supercapacitors, Journal of Materials Chemistry A, 3 (2015) 14445-14457.
[38] L.R. Merte, G. Peng, R. Bechstein, F. Rieboldt, C.A. Farberow, L.C. Grabow, W. Kudernatsch, S. Wendt, E. Lægsgaard, M. Mavrikakis, F. Besenbacher, Water-mediated proton hopping on an iron oxide surface, Science, 336 (2012) 889-893.
[39] A. Galińska, J. Walendziewski, Photocatalytic water splitting over Pt−TiO_2 in the presence of sacrificial reagents, Energy & Fuels, 19 (2005) 1143-1147.
[40] Y. Yang, J. Wen, J. Wei, R. Xiong, J. Shi, C. Pan, Polypyrrole-decorated Ag-TiO_2 nanofibers exhibiting enhanced photocatalytic activity under visible-light illumination, ACS Applied Materials & Interfaces, 5 (2013) 6201-6207.
[41] J. Yang, D. Wang, H. Han, C. Li, Roles of cocatalysts in photocatalysis and photoelectrocatalysis, Accounts of Chemical Research, 46 (2013) 1900-1909.
[42] H. Hou, M. Shang, F. Gao, L. Wang, Q. Liu, J. Zheng, Z. Yang, W. Yang, Highly efficient

photocatalytic hydrogen evolution in ternary hybrid TiO_2/CuO/Cu thoroughly mesoporous nanofibers, ACS Applied Materials & Interfaces, 8 (2016) 20128-20137.
[43] Y.-C. Chen, Y.-C. Pu, Y.-J. Hsu, Interfacial charge carrier dynamics of the three-component In_2O_3–TiO_2–Pt heterojunction system, The Journal of Physical Chemistry C, 116 (2012) 2967-2975.